Title: A multi-sill magma plumbing system beneath the axis of the East Pacific Rise

Authors: Milena Marjanović[1*], Suzanne M. Carbotte[1], Helene Carton[1], Mladen R. Nedimović[2,1], John C. Mutter[1], Juan Pablo Canales[3]

Affiliations:
[1] Lamont-Doherty Earth Observatory, Columbia University, Palisades, New York, USA
[2] Department of Earth Sciences, Dalhousie University, Halifax, Nova Scotia, Canada
[3] Woods Hole Oceanographic Institution, Woods Hole, Massachusetts, USA

*Correspondence to: Milena Marjanović, milena@ldeo.columbia.edu

The mid-crust axial magma lens detected at fast and intermediate spreading mid-ocean ridges[1-3] is believed to be the primary magma reservoir for formation of upper oceanic crust. However, the mechanism behind formation of the lower crust is a subject of ongoing debate. The sheeted sill model proposed from observations of ophiloites requires the presence of multiple lenses/sills throughout lower crust[4-8] but only a single lens is imaged directly beneath the innermost axial zone in prior seismic studies[1-3]. Here, high-fidelity seismic data from the East Pacific Rise reveal series of reflections below the axial magma lens that we interpret as mid-lower crustal lenses. These deeper lenses are present between 9°20-57′N at variable two-way-travel-times, up to 4.6 s (~1.5 km beneath the axial magma lens), providing direct support for the sheeted sill model[6,7]. From local changes in the amplitude and geometry of the events beneath a zone of recent volcanic eruption[9], we infer that melt drained from a lower lens contributed to the replenishment of the axial magma lens above and, perhaps, the eruption. The new data indicate that a multi-level sill complex is present beneath the East Pacific Rise that likely contributes to the formation of both the upper and lower crust.

Seismic studies of fast and intermediate spreading mid-ocean ridges (MOR) reveal a crustal magmatic system composed of a narrow (~1 km) axial magma lens (AML) located in the mid crust above a broader (4-6 km) crystal mush zone with 2-18% distributed melt extending into the lower crust[1-3,10]. While the AML is believed to be the primary magma source body for the dykes and lavas that make up the upper crust, the role of this melt body in the formation of the lower crustal gabbroic section is actively debated. In the "gabbro glacier" model most crystal growth occurs within the AML, which subsides by ductile flow to form the entire gabbro section[5]. In contrast, in the "sheeted sill" model, gabbro formation occurs *in situ* throughout the lower oceanic crust in small magma bodies, with the AML being the shallowest of these[6,7]. While the multiple sill model better explains observations of the layered gabbro section in ophiolites[4,6,7] and some geochemical characteristics of oceanic basalts[8], evidence for multiple sills has been lacking in seismic reflection studies at MOR. Lenses in the near-axis and off-axis lower crust have been detected[11,12] but magma sills directly beneath the AML have not been reported.

Here, we present multichannel seismic (MCS) data from the northern East Pacific Rise (EPR) that reveal mid-crustal seismic reflectors located below the AML (hereinafter referred to as sub-axial magma lens or SAML events). A series of multi-source, multi-streamer lines, resulting in up to 24 parallel reflection profiles spaced 37.5 m apart were collected along the ridge axis from 8º20′ to 10º10′N (Methods). These data were processed as individual 2D profiles, and collectively as a swath 3D volume. In addition, a series of across-axis lines spanning the ridge axis from ~9º37′-57′N were acquired for full 3D imaging. The most prominent SAML events are found between latitudes 9º20′ and 9º57′N (Figs 1, S1), where they appear as moderately bright discontinuous reflection events at two-way travel times (twtt) ranging from ~0.05 to 0.3 s below the AML. Below these brightest events, weaker and/or lower-frequency events are present at greater twtts, up to 4.6 s (Figs 1a-b, S1c, e).

Given the twtt range of the SAML events below the AML, there are several hypotheses that need to be ruled out for the origin of these events before interpretations in terms of real events from reflective horizons in the crust can be made. These include presence of a P-to-S converted phase from the AML ($P_{AML}S$), as well as returned energy associated with internal multiples, seafloor side scattering, or out-of-plane imaging of the AML or other crustal horizons. Strong converted shear waves reflected from an AML are expected when the melt content within the lens is high and are detected in prior studies using the method of partial-offset stacking[13,14]. Using a similar approach, a prominent $P_{AML}S$ event at twtts of ~0.2 s below the AML is observed in our data (Figs S2-S3), as predicted for this converted shear (Methods). This event is distinct from the SAML events in stacking velocity, frequency content, offset range at which it is observed in pre-stack data (Fig. S2), and in the twtt on stacked images.

Of the other, potential sources that could generate arrivals below the AML, simple intrabed and interbed multiples arising from energy reflecting within layer 2A and/or 2B (Figs S4-S5) can also be ruled out for all of the indicated SAMLs (Figs. 1a-b, S1; Supplementary Discussion). The SAML events do not show the expected consistent relationship with the presence and reflection intensity of the AML above and source-receiver offsets and travel-times for which SAML events are observed are inconsistent with those predicted for simple intrabed or interbed multiples (Figs S4-S6). Side-scatter arrivals from rough seafloor topography are present in places along our seismic sections, but occur at greater twtts (≥4.8 s) than the SAML events (Fig. S7). Furthermore, the SAML events are identified in the migrated 3D seismic volumes available for part of our study area ruling out side-echoes from possible out-of-plane AML events (Supplementary Discussion, Fig. S8).

Based on these considerations, we argue that the SAML events are P-wave reflections from horizons located beneath the AML. Could some of the SAML be previously undetected bottom reflections from a thick magma sill with the AML reflection arising from the top of this body? We consider this possibility unlikely. Using a range of geologically plausible velocities for the region below the AML (~4000-5500 m/s) (ref. 10) the estimated depths of the shallowest SAMLs range from ~100-800 m (for mapped twtt ~0.05-0.3 s) beneath the AML implying thick intracrustal sills. Prior waveform modelling of the AML reflection in this region[2,13-15] indicates that the magma lens is not more than 50 m thick, strongly arguing against the above possibility.

If these events are reflections off a magma body similar to the AML, is the material within them molten? The signal-to-noise ratio of the SAML events (even for the brightest ones) is too low for application of a standard AVO analysis[16]. Hence, to explore the nature of these sub-axial sills, we examine the amplitude versus offset (AVO) behaviour of SAML events on common-mid point (CMP) supergathers using a *quasi* forward AVO method[11,16] (Methods). The CMP supergather shows that the AVO response of the SAML event (when normalized) is similar to that of the AML event above it with comparable decrease in amplitude with increasing source-receiver offset (Fig. 2). In addition, the AVO response of the SAML event can be well approximated with simple 1D models calculated for a partially molten sill (with shear velocity within the sill of 800 m/s, see Methods).

From these analyses, we interpret the SAML events as reflections from thin magma sills similar to the AML, which vary in depth and character along the axis. The SAML events travel times locate them in the mid-crust, within the upper to mid gabbroic layer (up to 4.6 s, equivalent to 1200-1650 m below AML). We speculate that sills at even deeper levels may be present, but high seismic attenuation from melt presence in the overlying crust makes them invisible to our method (attenuation likely accounts for the weak amplitudes and lower frequency of the detected deeper SAMLs). These new seismic images indicate a multi-level, multi-body magma plumbing system beneath the inner axial zone of the EPR, in contrast to prior views of a single, axis centred mid-crustal melt sill above a broader crystal mush zone[3] and provide direct support for the sheeted sill model for the formation of the crust derived from ophiolite studies[e.g.,7].

Within the region of our seismic coverage, two mid-ocean ridge eruptions occurred, in 1991-92 (ref.17) and 2005-06 (ref.9,18), both centred at ~9°50′N, providing the opportunity to characterize the multi-sill magma source reservoir beneath the recent eruption (Fig. 1). Seismic data show that the AML is partitioned into three primary segments beneath the eruption, each defined by disruptions in the continuity of the AML reflection that coincide with local deepening of the event or small steps in travel-time from one lens segment to the next[19] (Fig. 1). The eruption products above each lens segment show distinct lava chemistry, eruptive volume and dominant flow morphology. The lava morphologies indicative of highest flow rate and the hottest (high MgO) lavas are both associated with the central lens segment between 9°48-51.5′N (ref. 20,21). Bright shallow SAML events are present beneath most of the eruption zone and reside at different twtts (from ~0.05-0.3 s) beneath each AML segment with steps in twtt of ~0.02-0.05 s from one segment to the next (Fig. 1). These SAML events weaken in reflection amplitude and disappear toward the northern and southern ends of the eruption zone as well as within a region extending ~3000 m along axis from ~9°49.9-51.4′N. This prominent "gap" in these shallow SAML events is present across the full ~700 m cross-axis width of the swath 3D volume and underlies the northern portion of the central AML segment. Estimates of the melt content of the AML derived from the presence of converted shear arrivals, waveform inversion, and AVO properties indicate, on average, less melt within the AML beneath this central eruption zone than to the north and south[14,22] (Fig. 1). In this same region, below the gap in the shallow SAML, a deeper dome-shaped, low-frequency SAML event (at ~4.33 s twtt) is observed, which is suggestive of a velocity “pull up” due to locally higher velocities in the rocks above (by >50-75 m/s, Fig. 1), which in this MOR setting could reflect less melt in the overlying crust.

We attribute this local zone of higher crystallinity within the AML, erased reflection signature of the SAML immediately below and locally increased seismic velocities, to evacuation of melt from both bodies during the 2005-06 eruption. In our proposed eruption scenario (Fig. 3), melts drained from a portion of the SAML ascended through the crust, possibly mixing with melts in the overlying central AML segment and erupted, contributing to the large eruption volumes and high flow rate morphologies observed at the seafloor. Geochemical studies of lavas from both the 1991-92 and 2005-06 eruptions lend further support to the interpretation that melts from below the AML contributed to the erupted lavas. Volatile concentrations in olivine melt inclusions from lavas sampled at ~9º50′N indicate that the source magmas for both eruptions underwent some crystallization at depths below the AML[23]. Furthermore, geochemical modelling of changes in lava compositions from the 1991-92 to 2005-06 eruptions indicate the source magmas for the more recent eruption were derived from the addition and mixing of more evolved melt from deeper in the crust, and not from simple fractional crystallization of the 1991 magma within the AML[21]. Recent studies of subaerial volcanic systems also provide evidence for magma transport from multiple levels within the crust during intrusion and eruption events. From the sequence of seismicity and eruptions observed during the 2010 Eyjafjallajökull eruption in Iceland, Tarasewicz et al.[24], infer that draining and depressurization of a shallow magma sill promoted mobilization of magma from deeper sills later in the eruption sequence. In a similar way, during the recent EPR eruptions, withdrawal of magmas from the AML may have led to tapping of melts from the underlying SAML and possibly deeper levels in the crust, contributing melts that differentiated at different depths to mix and erupt during a single eruption episode.

Methods:

Seismic survey and data processing. In summer 2008 a multi-streamer (four 6 km long streamers, each with 468 channels at 12.5 m spacing) and multi-source (two 3300 cu. in. air-gun arrays) seismic reflection survey was conducted aboard the *R/V Marcus G. Langseth* during expedition MGL0812[25]. One part of the survey was designed to image the axial zone of the EPR in the along-axis direction between 8º20′-10º10′N. North of 9º20′N, either two or three closely-spaced parallel sail lines were acquired over the ridge crest, including lines axis2r1 (acquired with 7.5 m streamer tow depth) and axis4 (10 m streamer tow depth) (Fig. 1). With the dual source and four-streamer configuration, each sail line yielded eight parallel common-mid point (CMP) lines spaced 37.5 m apart with an in-line CMP spacing of 6.25 m. The along-axis lines were processed along their entire lengths assuming a 2D geometry (using streamer 2 and combining shots from both airgun arrays), and as a 3D-binned swath for the region north of 9°20′N where multiple parallel lines were shot[22].

The processing sequence for the 2D sections and swath 3D volumes is similar and includes: trace editing, band-pass filter, spherical divergence correction and amplitude balancing, resampling to 0.004 s (with anti-aliasing filter applied), mute below the first water bottom multiple, velocity analysis, normal-move out (NMO) correction, stacking and Kirchhoff post-stack time migration. Geometry definition for the swath 3D processing involves identification of separate processing boxes to account for changes in survey line orientation of ~4º and number of CMP lines collected. Data are organized into 37.5×6.25 m^2 CMP bins and flexible binning is applied so that each CMP bin contains an equal number of traces corresponding to the nominal fold, here 39. 3D velocity functions for stacking and migration are constructed by interpolating between velocity functions determined for each 2D section hung from the seafloor bathymetry. Processing is conducted using *Paradigm's* processing suite *Focus*[22]. It is important to note that the collected 3D swath is narrower than required to properly migrate and image the AML and SAML events in cross-axis direction and hence the detailed plan view geometry of these events is not represented in the along-axis data.

In the final seismic sections and volumes, reflected arrivals from the seafloor and axial magma lens (AML) are imaged, as well as a series of events below the AML that are the focus of this study (Figs 1, S1). In addition, refracted arrivals from the steep velocity gradient zone at the base of layer 2A are observed at source-receiver offsets >1500 m and are stacked to provide an image of the base of layer 2A (ref. 26).

Stacking for $P_{AML}S$. In this study, partial offset stacking is used to identify S-wave converted phases from the AML ($P_{AML}S$) along line axis2r1. Pre-stack processing for optimal imaging of the $P_{AML}S$ phase includes band-pass filtering (2-7-20-40 Hz) and application of a dip filter in the f-k domain (dip pass: -0.0009 to 0.002 s/trace) on NMO-corrected (NMO velocity V=1520 m/s) 24 fold CMP supergathers (Fig. S2). After filtering and removing the above NMO, the CMP supergathers are split into single fold CMP gathers, NMO corrected using V_{RMS}=2400 m/s, and stacked for source-receiver offsets of 1500-4000 m (ref. 13, 14, 27) (Figs S2-S3).

AVO analysis. Due to the low signal-to-noise ratio of the SAML events in the pre-stack data, amplitude variation with offset (AVO) for these events is examined by calculating amplitude envelopes on CMP supergathers. For AVO analysis, we use a 24-fold CMP supergather centred at 19018 CMP with the same processing steps as for imaging the $P_{AML}S$ event (Fig. S2). After the initial dip filter described above, we apply a second dip filter with a reject-band between -0.002 to 0.002 s/trace to remove noise arising from shallow crustal events (low velocity) that remains at near offsets and partially masks the AML and SAML events. We assume that the dip filter has the same effect on both events and its application is considered appropriate. NMO correction (V=2600 m/s) is applied to the filtered CMP supergather and amplitude envelopes are calculated for the flattened AML and SAML events. Amplitude values are then picked from the amplitude envelopes, smoothed (using simple moving average) and plotted as a function of shot-receiver offset (for offsets from 500-4000 m; Fig. 2).

For comparison AVO response for the SAML event is normalized to the AML amplitude at minimum source-receiver offset. In addition, we calculate a range of theoretical AVO curves and normalize them to SAML amplitude at minimum offset. The theoretical curves are calculated using Zoeppritz equation for reflected P-wave[28] with velocities above SAML Vp_1=4500 m/s, Vs_1=2600 m/s and within SAML Vp_2=2400 m/s, and a range of shear velocities within the SAML of Vs_2=0; 800; and 1600 m/s.

Data Sources. MCS data are available through the Marine Geoscience Data System (MGDS) (http://www.marine-geo.org/tools/search/entry.php?id=MGL0812). Bathymetric data are from the GMRT Synthesis[29] available through the MGDS. Hydrothermal vent locations are from the Ridge2000 Data Portal of the MGDS at (http://www.marine-geo.org/portals/ridge2000/vents.php?feature_id=EPR).

2005-2006 lava flow outline[18] is from Soule, S. A., Interpretation of the Extent of the Axial Summit Trough and New Lava Emplaced during the 2005-2006 Eruption(s) at the East Pacific Rise 9ºN. Integrated Earth Data Applications (IEDA), doi:10.1594/IEDA/100071 (2012) and is available through the MGDS.

References:

1. Detrick R. S. *et al.* Multi-channel seismic imaging of a crustal magma chamber along the East Pacific Rise. *Nature* **326,** 35-42 (1987).

2. Kent, G. M., Harding, A. J. & Orcutt, J. A., Distribution of Magma Beneath the East Pacific Rise Between the Clipperton Transform and the 9°17′N Deval From Forward Modeling of Common Depth Point Data. *J. Geophys. Res.* **98,** 13,945–13,969 (1993).

3. Sinton, J. M. & Detrick, R. S., Mid-ocean ridge magma chambers. *J. Geophys. Res.* **97,** 197–216 (1992).

4. Nicolas A., Ceuleneer, G., Boudier, F. & Misseri, M., Structural mapping in the Oman ophiolites: Mantle diapirism along an oceanic ridge. *Tectonophysics* **151,** 27-56 (1988).

5. Phipps-Morgan, J. & Chen, Y. J., The genesis of oceanic crust magma injection, hydrothermal cooling, and crustal flow. *J. Geophys. Res.* **98,** 6283– 6297 (1993).

6. Boudier, F., Nicolas, A. & Ildefonse, B., Magma chambers in the Oman ophiolite: fed from the top and the bottom. *Earth Planet. Sci. Lett.* **144,** 239-250 (1996).

7. Kelemen, P. B., Kogu, K. & Shimizu, N., Geochemistry of gabbro sills in the crust – mantle transition zone of the Oman ophiolite: implications for the origin of the oceanic lower crust. *Earth Planet. Sci. Lett.* **146,** 475-488 (1997).

8. Natland, J. H. & Dick, H. J. B., Formation of the lower ocean crust and the crystallization of gabbroic cumulates at a very slowly spreading ridge. *J. Volcanol. Geother. Res.* **110**, 191-233 (2001).

9. Tolstoy, M., Waldhauser, F., Bohnenstiehl, D. R., Weekly R. T. & Kim W. -Y., Seismic identification of along-axis hydrothermal flow on the East Pacific Rise. *Nature* **451,** 181-184, (2008).

10. Dunn, R. A., Toomey, D. R. & Solomon, S. C., Three-dimensional seismic structure and physical properties of the crust and shallow mantle beneath the East Pacific Rise at 9°30'N. *J. Geophys. Res.* **105,** 23,537–23,555 (2000).

11. Canales, J. P., Nedimović, M. R., Kent, G. M., Carbotte S. M. & Detrick R. S, Seismic reflection images of a near-axis melt sill within the lower crust at the Juan de Fuca Ridge. *Nature* **460,** 89-93 (2009).

12. Canales, J. P. *et al.* Network of off-axis melt bodies at the East Pacific Rise. *Nature Geosci.* **5,** 279–283 (2012).

13. Singh, S. C., Kent, G. M., Collier, J. S., Harding, A. J. & Orcutt, J. A., Melt to mush variations in crustal magma properties along the ridge crest at the southern East Pacific Rise. *Nature* **394,** 874-878 (1998).

14. Xu, M. *et al.* Variations in axial magma lens properties along the East Pacific Rise (9°30′-10°00′N) from swath 3D seismic imaging and 1D waveform inversion. *J. Geophys. Res.,* **119,** 2721-2744, (2014).

15. Collier, J. S. & Singh, S. C., Detailed structure of the top of the melt body beneath the East Pacific Rise at 9°40′N from waveform inversion of seismic reflection data. *J. Geophys. Res.*, **102,** 20,287–20,304 (1997).

16. Nedimović, M. R. *et al.* Frozen melt lenses below the oceanic crust. *Nature* **436,** 1149-1152 (2005).

17. Haymon, R. M. *et al.* Volcanic eruption of the mid-ocean ridge along the East Pacific Rise crest at 9º45′-52′N: Direct submersible observations of the seafloor phenomena associated with an eruption event in April, 1991. *Earth Planet. Sci. Lett.* **119,** 85-101 (1993).

18. Soule, S. A., Fornari, D. J., Perfit, M. R. & Rubin, K. H., New insights into mid-ocean ridge volcanic processes from the 2005-2006 eruption of the East Pacific Rise, 9º46′-9º56′N. *Geology* **35,** 1079-1082 (2007).

19. Carbotte, S. M. *et al.* Fine-scale segmentation of the crustal magma reservoir beneath the modern eruptive zone of the East Pacific Rise. *Nature Geosci.* **6,** 866-870 (2013).

20. Fundis, A. T., Soule, S. A., Fornari, D. J., & Perfit, M. R., Paving the seafloor: Volcanic emplacement processes during the 2005–2006 eruptions at the fast spreading East Pacific Rise, 9°50′N. *Geochem. Geophys. Geosyst.* **11**, Q08024, (2010).

21. Goss, A. R. *et al.* Geochemistry of lavas from the 2005–2006 eruption at the East Pacific Rise, 9°46′N–9°56′N: Implications for ridge crest plumbing and decadal changes in magma chamber compositions. *Geochem. Geophys. Geosyst.* **11,** Q05T09, (2010).

22. Marjanović, M., Signatures of Present and Past Melt Distribution Along Fast and Intermediate Spreading Centers. *Ph.D Thesis, Columbia University*, New York, NY, USA, (2013).

23. Wanless, V. D. & Shaw, A. M., Lower crustal crystallization and melt evolution at mid-ocean ridges. *Nature Geosci.* **5,** 651-655, (2012).

24. Tarasewicz, J., White, R. S., Woods, A.W., Brandsdóttir B. & Gudmundsson M. T., Magma mobilization by downward-propagating decompression of the Eyjafjallajökull volcanic plumbing system. *Geophys. Reas. Lett.* **39,** L19309, (2012).

25. Mutter, J. C., Carbotte, S.M., Nedimović, N. R., Canales, J.P. & Carton, H., Seismic imaging in three dimensions on the East Pacific Rise. *Eos, Transactions American Geophysical Union,* Volume **90,** 374-375 (2009).

26. Harding, A. J., Kent, G. M. & Orcutt, J. A., A Multichannel Seismic Investigation of Upper Crustal Structure at 9°N on the East Pacific Rise: Implications for Crustal Accretion. *J. Geophys. Res.* **98,** 13,925–13,944 (1993).
27. Canales, J. P. *et al.* Seismic evidence for variations in axial magma chamber properties along the southern Juan de Fuca Ridge. *Earth Planet. Sci. Lett.* **246,** 353-366 (2006).

28. Guy, E.D., Radzevicius, S.J. & Conroy, J.P., Computer Programs for Application of Equations Describing Elastic and Electromagnetic Wave Scattering from Planar Interfaces. *Comput. Geosci.* **29,** 569-575 (2003).

29. Ryan, W.B.F. *et al.* Global Multi-Resolution Topography synthesis. *Geochem. Geophys. Geosyst.,* **10,** Q03014, (2009).

30. White, S. M., Haymon, R. M. & Carbotte, S. M., A new view of ridge segmentation and near-axis volcanism at the East Pacific Rise, 8-12ºN, from EM300 multibeam bathymetry. *Geochem. Geophys. Geosyst*. **7,** Q12O05, (2006).

Correspondence and request for materials should be addressed to M. M.

Acknowledgments

We thank Captain M. Landow, crew, and technical staff led by R. Steinhaus. We are also very grateful to Jeff Malloy, Douglas Foster and Charles Mosher from ConocoPhillips for comments and suggestions on the technical part of the paper. This research was supported by NSF awards OCE0327872 to J. C. M., S. M. C., OCE-0327885 to J. P. C., and OCE0624401 to M. R. N.

Author contributions

All authors participated in the MCS field experiment. M.M. carried out the MCS processing and data analysis. M.M. and S.M.C. interpreted the data and wrote the paper with contributions from all co-authors.

Competing financial interests

The authors declare no competing financial interests.

Figure legends:

Figure 1. Characteristics of the AML and sub-AML (SAML) seismic reflections imaged along the EPR. Along-axis seismic reflection profiles **a**, axis2r1 (dashed line shows location of the gather in Fig. 2) and **b**, axis4. **c**, Map of two-way-travel-time to the AML and **d**, the first SAML reflections below AML, both digitized from seismic data, and superimposed on EM300 bathymetry[30] in grey shaded relief. Black line in map view shows outline of 2005-06 lava flow[18]. Dotted and dashed lines show locations of axis2r1 and axis4, respectively. Black dot shows location of the gather in Fig. 2.

Figure 2. AVO behaviour of the AML and SAML. a, NMO corrected CMP supergather 19018 (location in Fig.1) including offsets to 4000 m. **b**, Filtered AVO response of AML and shallow SAML from the gather shown in **a** (Methods). For comparison, AVO response of the SAML is also shown normalized to AML. Theoretical AVO curves, normalized to AVO response of SAML are calculated using velocity models with a range of shear velocity within SAML of Vs_2=0-1600m/s (gray-shaded area). The theoretical AVO curve with Vs_2=800m/s is shown as the best fit to the AVO response of the SAML event.

Figure 3. Scenario for the 2005-06 eruption. During the eruption, compositionally distinct magmas intrude primarily vertically (broad arrows) from magma sill segments mapped directly below the eruption site[19,21] (top). After the eruption, the AML and SAML beneath the central eruption site are partially (AML cross-hatched pattern) to fully (SAML gap) crystallized due to draining of melt during the eruption (bottom). Presence of possible deeper SAMLs is marked by dashed outline.

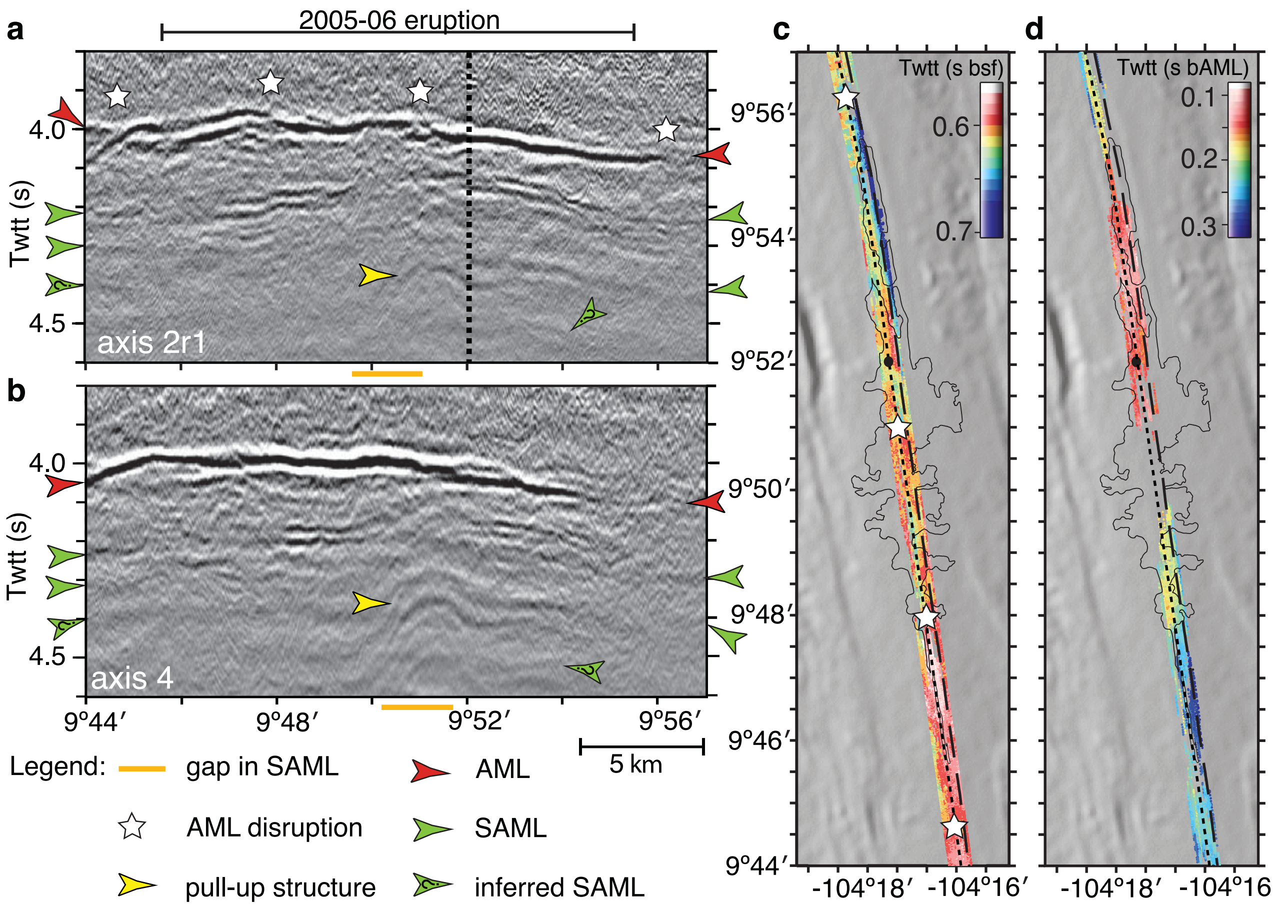

2005-06 eruption
a
b
c
d
Twtt (s)
4.0
4.5
axis 2r1
axis 4
9°44′
9°48′
9°52′
9°56′
5 km
Legend:
gap in SAML
AML disruption
pull-up structure
AML
SAML
inferred SAML
Twtt (s bsf)
0.6
0.7
Twtt (s bAML)
0.1
0.2
0.3
9°54′
9°50′
9°46′
-104°18′
-104°16′

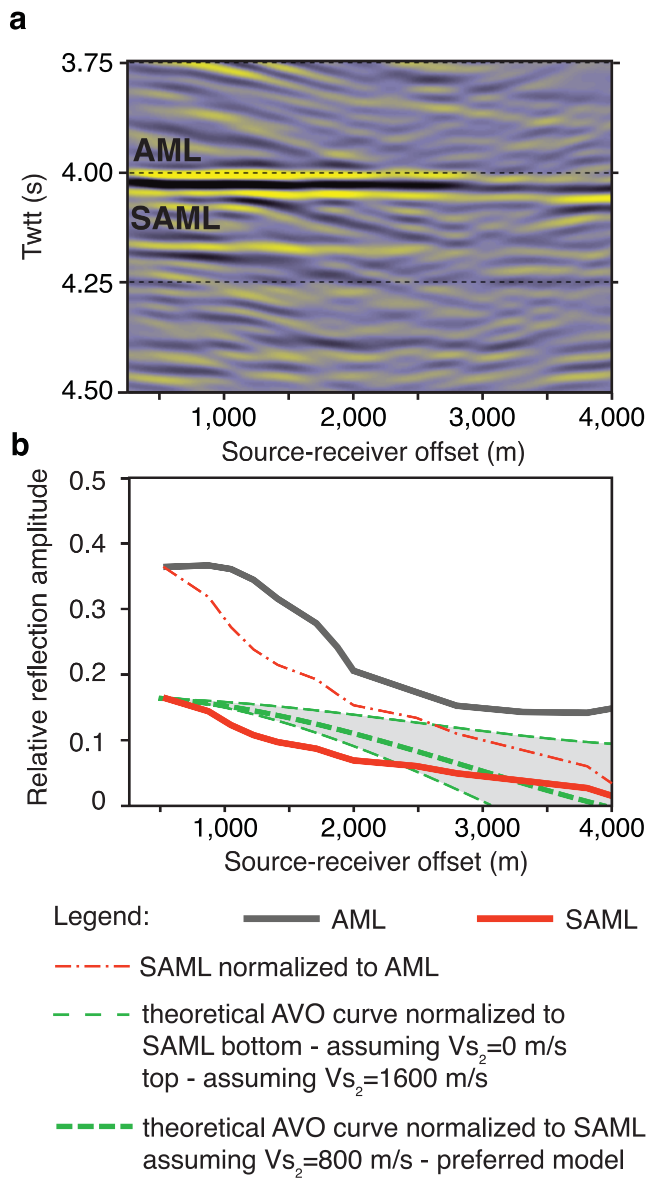
a
3.75
4.00
4.25
4.50
Twtt (s)
AML
SAML
1,000
2,000
3,000
4,000
Source-receiver offset (m)
b
0.5
0.4
0.3
0.2
0.1
0
Relative reflection amplitude
1,000
2,000
3,000
4,000
Source-receiver offset (m)
Legend:
AML
SAML
SAML normalized to AML
theoretical AVO curve normalized to SAML bottom - assuming Vs2=0 m/s top - assuming Vs2=1600 m/s
theoretical AVO curve normalized to SAML assuming Vs2=800 m/s - preferred model

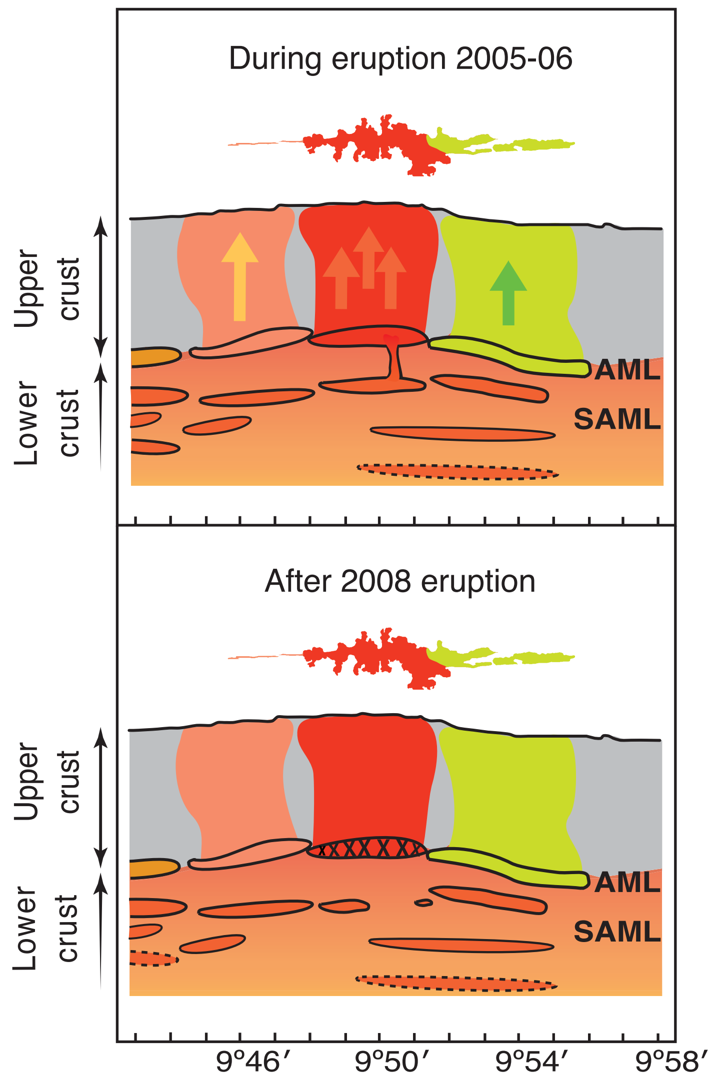
During eruption 2005-06
Upper crust
Lower crust
AML
SAML
After 2008 eruption
Upper crust
Lower crust
AML
SAML
9°46′
9°50′
9°54′
9°58′